Mon. Not. R. Astron. Soc. **391,** 164–177 (2008) doi:10.1111/j.1365-2966.2008.13676.x

An extensive photometric study of the Blazhko RR Lyrae star MW Lyr – I. Light-curve solution

J. Jurcsik,[1⋆] Á. Sódor,[1] Zs. Hurta,[1,2] M. Váradi,[1,3] B. Szeidl,[1] H. A. Smith,[4] A. Henden,[5] I. Dékány,[1] I. Nagy,[2] K. Posztobányi,[6] A. Szing,[7] K. Vida[1,2] and N. Vityi[2]

[1]*Konkoly Observatory of the Hungarian Academy of Sciences, PO Box 67,H-1525 Budapest, Hungary*
[2]*Department of Astronomy, Eötvös University, PO Box 49, H-1518 Budapest, Hungary*
[3]*Observatoire de Geneve, Universite de Genève, CH-1290 Sauverny, Switzerland*
[4]*Department of Physics and Astronomy, Michigan State University, East Lansing, MI 48824, USA*
[5]*American Association of Variable Star Observers, 49 Bay State Road, Cambridge, MA 02138, USA*
[6]*AEKI, KFKI Atomic Energy Research Institute, Thermohydraulic Department, PO Box 49, H-1525 Budapest 114, Hungary*
[7]*University of Szeged, Department of Exp. Physics and Astron. Obs., H-6720 Szeged, Dómtér 9, Hungary*

Accepted 2008 July 2. Received 2008 July 1; in original form 2008 May 16

ABSTRACT

We have obtained the most extensive and most accurate photometric data of a Blazhko variable MW Lyrae (MW Lyr) during the 2006–2007 observing seasons. The data within each 0.05 phase bin of the modulation period ($P_m = f_m^{-1}$) cover the entire light cycle of the primary pulsation period ($P_0 = f_0^{-1}$), making possible a very rigorous and complete analysis. The modulation period is found to be 16.5462 d, which is about half of that was reported earlier from visual observations. Previously unknown features of the modulation have been detected. Besides the main modulation frequency f_m, sidelobe modulation frequencies around the pulsation frequency and its harmonics appear at $\pm 2f_m$, $\pm 4f_m$ and $\pm 12.5f_m$ separations as well. Residual signals in the pre-whitened light curve larger than the observational noise appear at the minimum-rising branch-maximum phase of the pulsation, which most probably arise from some stochastic/chaotic behaviour of the pulsation/modulation. The Fourier parameters of the mean light curve differ significantly from the averages of the Fourier parameters of the observed light curves in the different phases of the Blazhko cycle. Consequently, the mean light curve of MW Lyr never matches its actual light variation. The Φ_{21}, Φ_{31} phase differences in different phases of the modulation show unexpected stability during the Blazhko cycle. A new phenomenological description of the light-curve variation is defined that separates the amplitude and phase (period) modulations utilizing the phase coherency of the lower order Fourier phases.

Key words: methods: data analysis – techniques: photometric – stars: horizontal branch – stars: individual: MW Lyr – stars: oscillations – stars: variables: other.

1 INTRODUCTION

The Blazhko modulation of RR Lyrae (RR Lyr) stars, a phenomenon known for about a century, is still one of the open questions in astrophysics. The problems and the inconsistencies of the existing models with observational facts were recently discussed in details by Stothers (2006), therefore we only briefly mention here that none of the suggested models (magnetic oblique rotator, Shibahashi 2000; resonant excitation of non-radial modes, Dziembowski & Mizerski 2004) can explains the complexity of all the observed properties of the modulation.

Alternatively, Stothers (2006) suggests that the modulation may be explained by continuous amplitude and period changes of the pulsation due to the action of a turbulent convective dynamo in the lower envelope of the star, with dynamo cycle identical with the Blazhko period. This explanation does not involve any non-radial mode component, the phenomenon is interpreted in the framework that Blazhko RRab stars are purely fundamental mode radial pulsators. However, Stothers (2006) gives only a qualitative, rough picture of his model, that have to be checked both observationally and theoretically, thus the investigation of the phenomenon still remains an important and valid task.

⋆E-mail: jurcsik@konkoly.hu

A lot of efforts have been already made in studying the light curve changes of RR Lyr stars but most of the available photometries of Blazhko variables have some defects: inaccuracy (visual, photographic data), biased data sampling (the photoelectric observations focused mostly on the rising branch, maximum phase of the light curve), data inhomogeneity due to rare data sampling on a too long time-base (the time-scale of period changes and changes in the modulation properties can be as short as a few years) etc. Most of the recent CCD and/or photoelectric observations of individual Blazhko stars are not extended enough to study the modulation properties in full detail. The first multicolour photometric data that covered each phase of both the modulation and the pulsation within a short time-base (one season) were published for RR Gem (Jurcsik et al. 2005). During the period of the CCD observations RR Gem showed, however, small amplitude modulation, that limits the available information due to the low signal-to-noise ratio (S/N) of the modulation signals.

We started a systematic search for previously unknown Blazhko variables at Konkoly Observatory in 2004 using the advantage of full access to an automated 60-cm telescope (Sódor 2007). The aim has also been to clear up questionable cases. In Sódor & Jurcsik (2005) we have revised the list of known Blazhko variables (Smith 1995). The modulation of MW Lyrae (MW Lyr) was found to be ambiguous as the photographic observations (Gessner 1966) did not confirm the modulation detected in visual data by Mandel (1970). Our CCD observations of MW Lyr affirm the light-curve modulation of the star, but with a modulation period about half of that Mandel (1970) announced.

Spectroscopic observation of MW Lyr has never been obtained, however, based on its short period ($P_{\rm puls} = 0.397$ d), it should be a relatively hot and metal-rich RR Lyr star.

In the 2006 and 2007 seasons we obtained CCD photometric observations of MW Lyr ($\alpha = 18^{\rm h}19^{\rm m}53\overset{\rm s}{.}8$, $\delta = +31^\circ58'54''$, J2000). This is the first multicolour photometric data set of a large modulation amplitude Blazhko variable that is condensed, extended and accurate enough to detect previously unknown properties of the modulation.

In this paper the photometric data of MW Lyr are published and analysed. The light-curve solution (frequency analysis) is discussed using mostly the *V*-band data. A second paper is going to be devoted to the study of the colour behaviour during the course of the modulation cycle.

2 DATA

The major part of the observations were obtained with the automated 60-cm telescope of the Konkoly Observatory, Svábhegy, Budapest, equipped with a Wright Instruments 750 × 1100 CCD camera (FoV 17 × 24 arcmin^2). Measurements were taken on 177 nights between 2006 May and 2007 July. CCD observations with the 60-cm telescope of the Michigan State University equipped with an Apogee Ap47p CCD camera (FoV 10 × 10 arcmin^2) and with the 1-m RCC telescope of the Konkoly Observatory equipped with a Princeton Instruments VersArray 1300B CCD camera (FoV 6 × 6 arcmin^2) were obtained on six and three additional nights in 2006 July and in 2007 August, respectively. Johnson–Cousins $BVI_{\rm C}$ filters were used in all the observations. Altogether 5700–5800 data points in the $BVI_{\rm C}$ passbands were gathered. Observations in $R_{\rm C}$ band were also obtained on 15/3 nights with the Konkoly 60/100 cm telescopes.

Data reduction was performed using standard IRAF[1] packages. Aperture photometry of MW Lyr and several neighbouring stars were carried out. In the analysis magnitudes of MW Lyr relative to GSC2.2 N0223233663 (C0) are used. Table 1 lists the basic data and Fig. 1 shows the positions of our comparison and check stars. The magnitude differences of the comparison and check stars remained constant within 0.010–0.015, 0.009–0.013, 0.008–0.012, 0.009–0.013 mag in the $B, V, R_{\rm C}$ and $I_{\rm C}$ bands, respectively (see also Fig. 7).

Transformation to the standard system was done using the $B, V, R_{\rm C}$ and $I_{\rm C}$ magnitudes of the stars in the field of MW Lyr observed by A. Henden with the USNO Flagstaff Station 1.0-m telescope equipped with a SITe/Tektronix 1024 × 1024 CCD. A complete list of the positions and standard $BV(RI)_{\rm C}$ magnitudes of these stars are available online as Supplementary Material (Table S1). To calculate the colour terms of the transformations the nightly instrumental *V* and *B* light curves were fitted by different order Fourier sums to determine the *V* magnitudes at the moments of the $B, R_{\rm C}, I_{\rm C}$ observations and the *B* magnitudes at the moments of the *V* observations. No transformation was applied in the $I_{\rm C}$ band of the Konkoly 60-cm data as no colour dependency of the differences between the instrumental and standard magnitudes was found in this band.

Taking into account the proximity of the comparison star to the variable only second-order extinction correction were applied in the *B* band.

$B - V, V - R_{\rm C}$ and $V - I_{\rm C}$ colours were derived utilizing the *V* observations and fitted values of the $B, R_{\rm C}, I_{\rm C}$ curves according to nightly Fourier fits for the moments of the *V* measurements. Differential *V* magnitudes and $B - V, V - R_{\rm C}$ and $V - I_{\rm C}$ colours of MW Lyr with respect to C0 are given in Table 2. The heliocentric Julian Date, $\Delta V, \Delta(B - V), \Delta(V - R_{\rm C})$ and $\Delta(V - I_{\rm C})$ relative magnitudes and the observatory ID are given in columns 1–6, respectively. The entire list of photometric data is available online as Supplementary Material. In Tables S2a, S2b and S2c (online only) the $\Delta B, \Delta R_{\rm C}$ and $\Delta I_{\rm C}$ time series are given.

Maximum timings and maximum brightness values of the *V* data set were determined for 88 epochs (Table 3). The complete list of these data is available online.

3 RESULTS

The *V* light curve of MW Lyr and the data folded with the pulsation and modulation periods are shown in Fig. 2. The light curve is strongly modulated, the full amplitudes of the amplitude and phase modulations are larger than 0.45 mag and 0.07 phase of the pulsation (∼40 min), respectively (see also Fig. 9). The modulation seems to have larger amplitude at around minimum and rising branch phases than at maximum light as Fig. 3 shows. In this figure the residual light curve is phased with the pulsation period after the pulsation components are removed. The large amplitude of the residuals around minimum phase is the consequence of the large amplitude of the phase modulation. In reality, the amplitude of the maximum brightness variation is larger than the amplitude of the minimum brightness variation as the top and bottom envelope curves of panel C in Fig. 2 show.

[1] IRAF is distributed by the National Optical Astronomy Observatory, which is operated by the Association of Universities for Research in Astronomy, Inc., under cooperative agreement with the National Science Foundation.

Table 1. Data of comparison and check stars.

Name	GSC2.2 ID	USNO-B1.0 ID	Coord		V (mag)[a]	$B-V$ (mag)[a]	$V-R_C$ (mag)[a]	$V-I_C$ (mag)[a]
			RA	Dec.				
C0	N0223233663	1219-0328347	18 19 56.80	+31 58 13.3	11.841	0.582	0.315	0.666
C1	N0223233659	1219-0328429	18 20 06.56	+31 58 56.4	12.986	0.682	0.383	0.788
C2	N0223233671	1219-0328258	18 19 48.61	+31 57 14.6	13.921	0.858	0.480	0.950
C3	N02232332613	1219-0328267	18 19 48.91	+31 56 54.4	14.363	0.603	0.338	0.671

[a]Standard magnitudes measured by A. Henden.

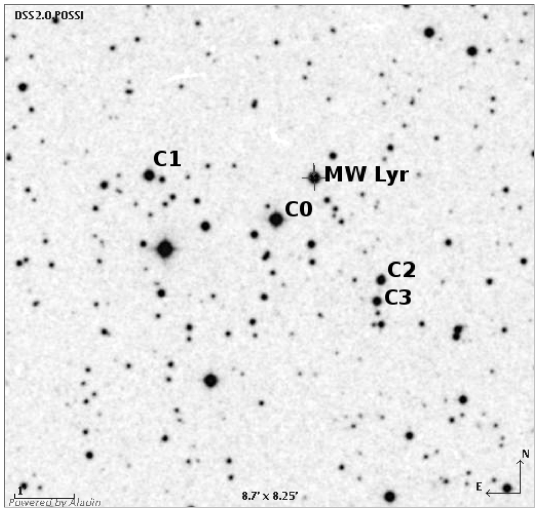

Figure 1. Map of MW Lyr and the comparison (C0) and check stars (C1, C2 and C3).

Table 2. Time series of the V magnitude and colour differences of MW Lyr relative to the comparison star C0 (the full table is available online).

HJD 240 0000	ΔV	$\Delta(B-V)$	$\Delta(V-R_C)$	$\Delta(V-I_C)$	Obs[a]
53887.34009	2.218	−0.075	−0.064	−0.041	1
53887.35249	2.227	−0.073	−0.035	−0.035	1
53887.35867	2.250	−0.087	−0.020	−0.020	1
53887.36489	2.257	−0.085	−0.020	−0.023	1
...	...	...	...	...	....

[a]1 – Konkoly 60 cm; 2 – MSU 60 cm; 3 – Konkoly 1 m.

Table 3. Maximum timings and brightness values derived from the V light curve (the full table is available online).

Maximum time HJD 240 0000	V maximum brightness relative magnitude to C0
53887.520	1.501
53901.447	1.285
53903.428	1.480
...	...

The elements of the pulsation and modulation are

$$T_{\max\,\mathrm{puls}} = 245\,3963.4950\,[\mathrm{HJD}] + 0.3976742\,E_{\mathrm{puls}}$$

and

$$T_{\max\,\mathrm{Bl}} = 245\,3963.4950\,[\mathrm{HJD}] + 16.5462\,E_{\mathrm{Bl}}.$$

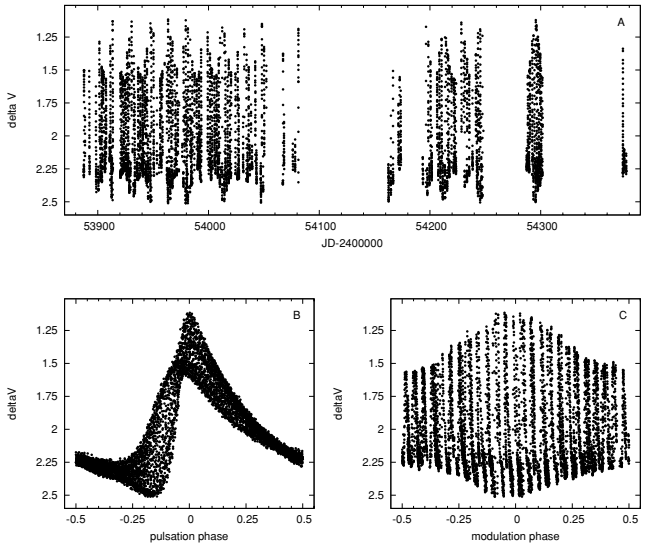

Figure 2. Delta V magnitudes versus Julian Date (panel A), data phased with the 0.397674 d pulsation (panel B) and the 16.546 d modulation periods (panel C) are shown.

The pulsation and modulation periods are those that yield the best fit to the V light curve with the pulsation (kf_0) and modulation ($kf_0 \pm f_m, kf_0 \pm 2f_m, f_m$ and $2f_m$) frequency components using 'locked' frequency solution (i.e. the modulation components are at the positions of the linear combination frequencies). Details of the frequency component determinations are given in Section 3.1.

Data analysis was performed using the different applications of the MUFRAN/TIFRAN packages (Kolláth 1990; Kolláth & Csubry 2006), a linear combination fitting program developed by Á. Sódor, and the linear and non-linear curve fitting abilities of gnuplot.[2]

3.1 The light-curve solution

The Fourier spectrum of Blazhko RRab stars is characterized by equidistant frequency triplets with frequency separation identical with the modulation frequency (see e.g. Smith et al. 1999; Jurcsik et al. 2005; Kolenberg et al. 2006). In the residual spectrum of RV UMa, equidistant quintuplets were identified by Hurta et al. (2008). The appearance of the modulation frequency (f_m) itself was a matter of debate for long, but in the spectra of extended and accurate data sets f_m also shows up unquestionably (Jurcsik et al. 2005, 2006; Hurta et al. 2008).

The Fourier spectrum of MW Lyr is also dominated by these frequency components. Pulsation frequencies appear up to the 12th

[2] http://www.gnuplot.info/

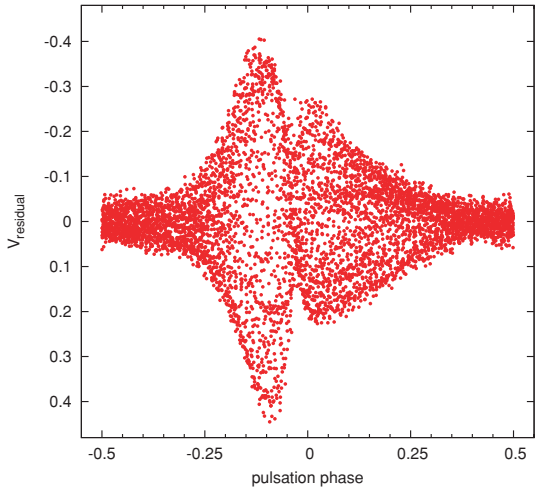

Figure 3. Residual V light curve of MW Lyr after removing the pulsation components of the light-curve solution from the data. The residuals have larger amplitude at around the minimum, rising branch phases of the pulsation than around maximum brightness due to the large amplitude of the phase modulation.

order, while the $kf_0 + f_m$ and $kf_0 - f_m$ components are present with $k \leq 13$ and $k \leq 10$, respectively. The modulation frequency (f_m) has an amplitude of 0.014 mag in the V data, which is as high as the amplitude of the sixth harmonic component of the pulsation. Pre-whitening the data with the frequencies of the triplet solution significant peaks in the residual spectrum appear, indicating that the light curve cannot be accurately fitted simply with equidistant frequency triplets.

Fig. 4 shows the residual spectra of the V data in the 0–20 cd^{-1} frequency range and in the vicinity of the kf_0 ($k = 1, \ldots, 7$) pulsation frequencies after pre-whitening with different frequency solutions. Table 4 summarizes the frequency solutions applied as more and more frequency components are identified. All the identified frequency components (pulsation plus modulation frequencies) are simultaneously fitted to the original data and this light-curve solution is used in the next step of the analysis. In Section 3.3 it is documented that the simultaneous fit of all the frequency components gives better light-curve solution than if the frequency components are successively fitted and are removed from the data in consecutive steps.

The left-hand panels of Fig. 4 show the residual spectrum after removing the triplet frequency solution (solution A). The highest peaks appear at $kf_0 + 2f_m$ frequencies. The $kf_0 - 2f_m$ and the $2f_m$ frequencies are also detected but with relatively small amplitudes. There are altogether 16 frequencies identified to belong to the $kf_0 \pm 2f_m$ modulation series. Fitting the data with the quintuplet frequencies (solution B) the residual spectrum (middle panels in Fig. 4) is still not flat, besides other peaks two sets of frequencies are evident, one at $4f_m$ and the other at $12.5f_m$ frequency separations. Unfortunately, the frequencies of these series are very close to the ± 1 cd^{-1} alias components of each other (see their frequency values in Table 5), that makes the determination of the amplitudes of these components ambiguous. However, either the $kf_0 \pm 4f_m$ or the $kf_0 \pm 12.5f_m$ components are removed, members of the other frequency series remain, consequently the components of the $kf_0 \pm 4f_m$ and the $kf_0 \pm 12.5f_m$ frequency series are independent signals. In the right-hand panels in Fig. 4 it is shown that even if the septuplet solution is removed with five components of the $kf_0 \pm 4f_m$ series (solution C), signals at $12.5f_m$ separations are still present in the residual. These are the highest peaks detected in this spectrum. It is not at all clear whether these modulation components are indeed connected to the main modulation frequency or it happens just by chance that this secondary modulation has a modulation frequency very close to $12.5\,f_m$. We can only say that the frequencies of this modulation series are within the uncertainties at the positions of $kf_0 \pm 12.5f_m$. If the frequencies of these modulation components are not locked to the $kf_0 \pm 12.5f_m$ positions in the fitting process their displacements do not exceed significantly and/or systematically the displacements of the other modulation frequency components with similar amplitude (see data in Table 5).

Some of the other peaks in the residual of the septuplet solution also form series with common frequency separation from the pulsation components. There are remaining peaks very close to the pulsation components at $f_0 - f'_m, 2f_0 - f'_m, 3f_0 - f'_m$ and f'_m frequencies with $f'_m = 0.00197$ cd^{-1}. The periods and amplitudes of these frequency components are somewhat uncertain as this modulation period is $\sim$500 d, hardly shorter than the total length of the observations. These components can be identified either with an additional long period modulation or with residuals caused by slight changes of the pulsation period during the observations.

In light-curve solution D, besides the quintuplet frequencies, the $kf_0 \pm 12.5f_m$ and the f'_m modulation components are also fitted and removed. In Fig. 5 the residual spectra of the B, V and I_C observations are shown after pre-whitening with light-curve solution D. These residual spectra are characterized with a broad-band low-frequency signal centred on about the pulsation frequency and with series of further modulations at e.g. $-3f_m, 5f_m, -11.5f_m$ and $13.5f_m$ frequencies. There are also further frequency peaks in the ± 0.15 cd^{-1} vicinity of the f_0 pulsation frequency. Though the S/N of the amplitudes of many of these frequency components are larger than 3, we stop frequency identification at this level as the addition of these frequency components does not improve the light-curve solution significantly.

In Table 5 details of light-curve solution D are given for the B, V and I_C data. Column 1 gives the identification of the frequencies, Column 2 lists the frequencies of the 'locked' frequency solution (exact linear combinations of the pulsation and modulation components). The next three columns give the differences in the frequency values (Δf) of the 'let free' solutions for the B, V and I_C light curves. In the let free solutions only the harmonic components of the pulsation are at locked frequency values but the best frequency values of f_0 and all the modulation frequency components are searched in a non-linear process. For comparison purposes, $\Delta f/\sigma_f$ are given in columns 6–8 in the three bands. The σ_f error estimates of the frequencies are calculated using the formula given by Montgomery & O'Donoghue (1999). It is important to note here that, in the case of correlated noise, these errors underestimate the true uncertainties of the frequencies significantly. For most of the identified modulation frequency components the frequency displacements are 0.5–4.0 times the calculated σ_f values.

Frequency components with larger displacements ($\Delta f/\sigma_f > 3$) in each band are

f_m ($V_{amp} = 0.014$); $\Delta f(V) = 0.00011$ cd^{-1},

$f_0 + 2f_m$ ($V_{amp} = 0.004$); $\Delta f(V) = -0.00055$ cd^{-1},

$4f_0 - 2f_m$ ($V_{amp} = 0.003$); $\Delta f(V) = -0.00064$ cd^{-1},

$f_0 - 4f_m$ ($V_{amp} = 0.003$); $\Delta f(V) = 0.00041$ cd^{-1},

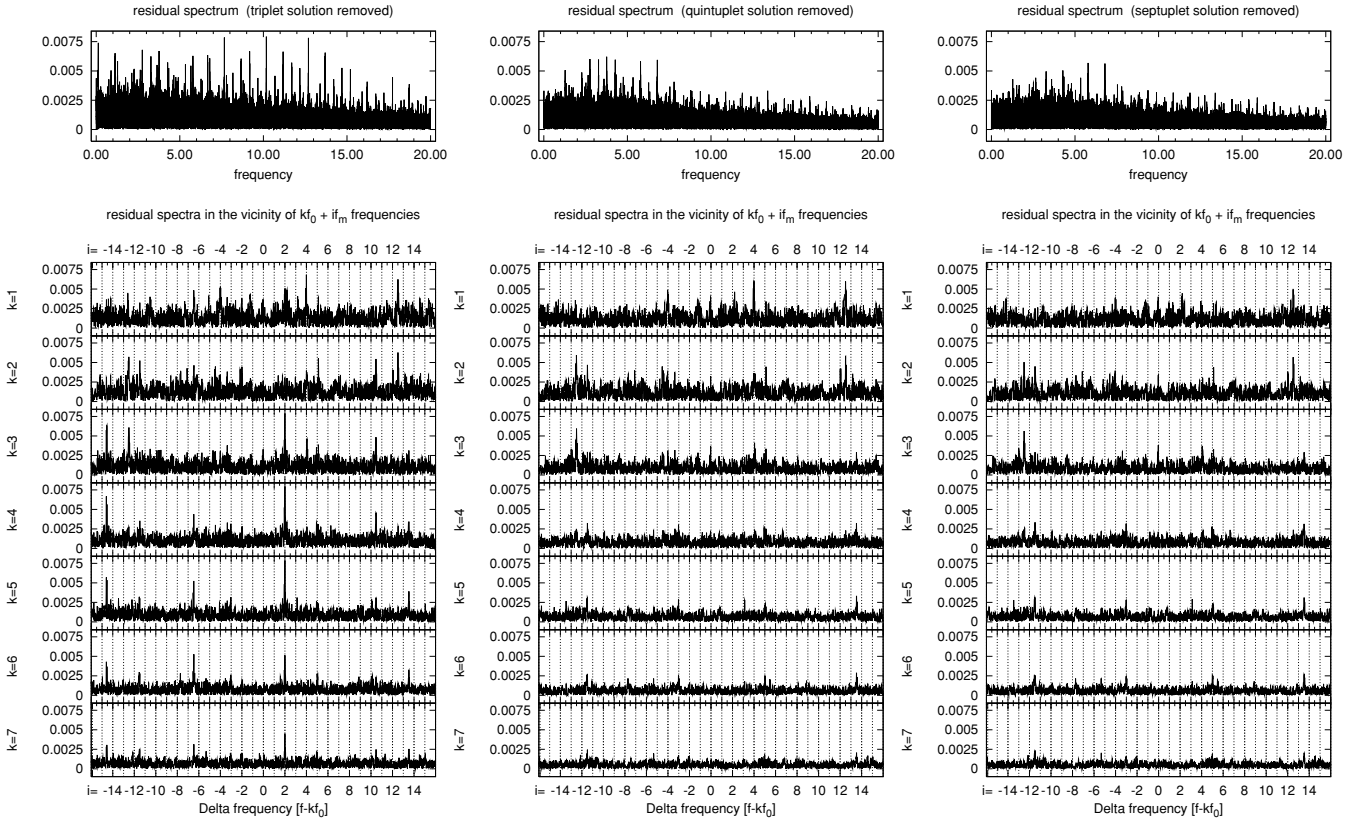

Figure 4. Residual spectra (top panels) and spectra in the vicinity of the $kf_0, k = 1, \ldots, 7$ pulsation frequency components (bottom panels) are drawn. In these panels $\sim$2 cd^{-1} frequency ranges are enlarged. On the x-axis ticks are at $2f_{\rm m}$ separation, 0 corresponds to the positions of kf_0. For the sake of lucidity a grid with $if_{\rm m}$ spacing is also drawn. In the left-hand panels residuals after pre-whitening with the triplet frequency solution (solution A) are shown. The highest peaks in the spectrum appear at $kf_0 + 2f_{\rm m}$ frequencies. The $kf_0 - 2f_{\rm m}$ frequencies do not evidently show up in these spectra but in later steps of the pre-whitening some of these components also emerge with S/N larger than 3. Residuals after pre-whitening with the quintuplet frequency solution (solution B) are shown in the middle panels. The highest peaks appear at $kf_0 \pm 4f_{\rm m}$ and $kf_0 \pm 12.5f_{\rm m}$ frequencies. These two series of modulation components are unfortunately seriously biased as they are very close to the $\pm$1 cd^{-1} alias components of each other. However, after pre-whitening the data also with five frequencies of the $kf_0 \pm 4f_{\rm m}$ components (septuplet: solution C) as shown in the right-hand panels, it becomes evident that the $kf_0 \pm 12.5f_{\rm m}$ components still remain in the spectrum. We conclude, therefore, that they are real frequencies, indeed, and not alias artefacts of the data sampling. There are other well defined frequency series appearing with common frequency separations, too. One is very close to the pulsation components at $f'_{\rm m} = 0.0019$ cd^{-1} separation. Four components of this series can be identified: $f_0 - f'_{\rm m}, 2f_0 - f'_{\rm m}, 3f_0 - f'_{\rm m}$ and $f'_{\rm m}$. In light-curve solution D the septuplet and the $kf_0 \pm 12.5f_{\rm m}$ modulation and also modulation components with $f'_{\rm m} = 0.00197$ cd^{-1} separation are removed. The residuals of light-curve solution D are shown in Fig. 5.

Table 4. Light-curve solutions.

Solution	No. of frequencies	Frequency identification
A (triplet)	36	$kf_0, k = 1, \ldots, 12; kf_0 - f_{\rm m}, k = 1, \ldots, 10; kf_0 + f_{\rm m}, k = 1, \ldots, 13; f_{\rm m}$
B (quintuplet)	53	Frequencies in solution A and $kf_0 - 2f_{\rm m}, k = 1, \ldots, 7; kf_0 + 2f_{\rm m}, k = 1, \ldots, 9; 2f_{\rm m}$
C (septuplet)	58	Frequencies in solution B and $kf_0 - 4f_{\rm m}, k = 1, 2, 3; kf_0 + 4f_{\rm m}, k = 1, 2$
D	66	Frequencies in solution C and $kf_0 - 12.5f_{\rm m}, k = 2, 3; kf_0 + 12.5f_{\rm m}, k = 1, 2; kf_0 - f'_{\rm m}, k = 1, 2, 3; f'_{\rm m}$
E	96	Frequencies in solution D and 30 additional frequencies (see details in the text)

Note. $f_0 = 2.514\,621$ cd^{-1}; $f_{\rm m} = 0.060\,437$ cd^{-1}; $f'_{\rm m} = 0.00\,197$ cd^{-1}.

$3f_0 - 4f_{\rm m}$ ($V_{\rm amp} = 0.002$); $\Delta f(V) = 0.00090$ cd^{-1},

$f_{\rm m}$ ($V_{\rm amp} = 0.002$); $\Delta f(V) = 0.00196$ cd^{-1}.

The larger uncertainty of the $f_{\rm m}$ component arises simply from the fact that this modulation period is hardly shorter than the time-span of the observations. The larger displacements of the $4f_{\rm m}$ components are most probably due to their strong $\pm$1 cd^{-1} alias connections with the frequencies of the $12.5f_{\rm m}$ modulation series. The reason why the frequency displacement of the other three modulation components is unexpectedly large is unknown. Based on the data given in Table 5, we think that there is no serious reason to assume that the modulation frequencies are not, in fact, at their 'locked' positions.

In columns 9–14 of Table 5 the amplitudes and phases of the B, V and $I_{\rm C}$ light curves according to sine term decomposition are given. Frequencies with S/N (S/N is defined as the ratio of the V amplitude and the mean value of the residual spectrum of light-curve solution

Table 5. Fourier parameters of light-curve solution D in the B, V, I_C bands.

Frequency ID	Frequency (cd^{-1})	$\Delta f(B)$	$\Delta f(V)$ (10^{-5} cd^{-1})	$\Delta f(I_C)$	$\Delta f/\sigma_f$ B	$\Delta f/\sigma_f$ V	$\Delta f/\sigma_f$ I_C	$A(B)$ (mag)	$\Phi(B)$ (rad)	$A(V)$ (mag)	$\Phi(V)$ (rad)	$A(I_C)$ (mag)	$\Phi(I_C)$ (rad)
f_0	2.514 621	0.14	0.39	0.56	2.0	4.2	3.7	0.4998	1.963	0.3741	1.919	0.2302	1.772
$2f_0$	5.029 242	–	–	–	–	–	–	0.2063	6.211	0.1585	6.200	0.1006	6.152
$3f_0$	7.543 863	–	–	–	–	–	–	0.0968	4.366	0.0759	4.354	0.0500	4.335
$4f_0$	10.058 484	–	–	–	–	–	–	0.0469	2.323	0.0373	2.334	0.0251	2.317
$5f_0$	12.573 105	–	–	–	–	–	–	0.0242	0.305	0.0199	0.268	0.0138	0.268
$6f_0$	15.087 726	–	–	–	–	–	–	0.0165	4.446	0.0139	4.388	0.0093	4.389
$7f_0$	17.602 347	–	–	–	–	–	–	0.0117	2.360	0.0096	2.394	0.0069	2.332
$8f_0$	20.116 968	–	–	–	–	–	–	0.0093	0.324	0.0074	0.294	0.0049	0.368
$9f_0$	22.631 589	–	–	–	–	–	–	0.0065	4.670	0.0055	4.696	0.0039	4.574
$10f_0$	25.146 210	–	–	–	–	–	–	0.0053	2.735	0.0039	2.856	0.0025	2.592
$11f_0$	27.660 831	–	–	–	–	–	–	0.0031	0.974	0.0028	0.788	0.0022	0.940
$12f_0$	30.175 452	–	–	–	–	–	–	0.0024	5.215	0.0018	5.329	0.0010	5.384
f_m	0.060 437	8.87	10.95	14.93	4.9	4.4	4.3	0.0193	3.628	0.0140	3.635	0.0100	3.558
$f_0 + f_m$	2.575 058	0.06	0.26	−0.04	0.2	0.7	−0.1	0.1217	3.316	0.0900	3.332	0.0559	3.352
$2f_0 + f_m$	5.089 679	0.83	0.27	0.24	2.6	0.6	0.3	0.1067	1.402	0.0805	1.436	0.0506	1.501
$3f_0 + f_m$	7.604 300	0.73	0.57	0.83	1.4	0.8	0.8	0.0648	6.013	0.0502	6.036	0.0324	6.103
$4f_0 + f_m$	10.118 921	3.17	1.87	2.58	4.1	1.9	1.7	0.0451	4.316	0.0357	4.329	0.0231	4.352
$5f_0 + f_m$	12.633 542	2.27	2.94	4.63	1.8	1.9	1.9	0.0274	2.502	0.0219	2.497	0.0142	2.491
$6f_0 + f_m$	15.148 163	9.30	6.38	5.81	4.4	2.3	1.4	0.0165	0.533	0.0126	0.513	0.0085	0.525
$7f_0 + f_m$	17.662 784	6.96	4.21	12.06	2.0	1.0	1.9	0.0098	4.765	0.0085	4.762	0.0054	4.763
$8f_0 + f_m$	20.177 405	11.58	5.22	5.85	2.3	0.8	0.6	0.0069	2.584	0.0054	2.627	0.0033	2.676
$9f_0 + f_m$	22.692 026	6.93	0.33	−8.80	1.2	0.0	−0.6	0.0058	0.627	0.0042	0.595	0.0024	0.721
$10f_0 + f_m$	25.206 647	−9.99	9.96	13.16	−1.2	1.0	0.8	0.0041	4.919	0.0035	4.798	0.0022	5.023
$1f_0 + f_m$	27.721 268	−13.31	19.24	28.54	−1.2	1.7	1.4	0.0031	2.820	0.0030	2.894	0.0016	2.586
$12f_0 + f_m$	30.235 889	13.97	2.98	65.67	1.1	0.2	1.8	0.0027	0.681	0.0020	0.987	0.0010	0.608
$13f_0 + f_m$	32.750 510	−9.57	11.16	14.54	−0.6	0.4	0.4	0.0020	5.425	0.0014	5.563	0.0010	5.074
$f_0 - f_m$	2.454 184	3.30	3.74	2.69	6.2	5.2	2.3	0.0650	4.770	0.0486	4.787	0.0299	4.835
$2f_0 - f_m$	4.968 805	0.33	2.23	0.52	0.6	2.9	0.4	0.0599	2.731	0.0451	2.775	0.0278	2.864
$3f_0 - f_m$	7.483 426	1.87	3.54	3.48	2.3	3.4	2.0	0.0426	1.094	0.0331	1.109	0.0204	1.161
$4f_0 - f_m$	9.998 047	−1.28	0.38	−1.02	−1.1	0.2	−0.4	0.0287	5.476	0.0225	5.534	0.0144	5.575
$5f_0 - f_m$	12.512 668	4.19	0.38	−1.26	2.2	0.2	−0.3	0.0184	3.804	0.0141	3.763	0.0094	3.801
$6f_0 - f_m$	15.027 289	−4.38	2.83	−6.53	−1.7	0.8	−1.2	0.0132	1.829	0.0094	1.770	0.0066	1.768
$7f_0 - f_m$	17.541 910	6.88	−1.57	3.95	1.6	−0.3	0.5	0.0081	6.253	0.0070	6.239	0.0047	6.097
$8f_0 - f_m$	20.056 531	−19.32	−14.07	−3.38	−2.8	−1.7	−0.3	0.0049	4.436	0.0042	4.422	0.0026	4.392
$9f_0 - f_m$	22.571 152	−31.04	−21.41	−5.76	−2.5	−1.5	−0.3	0.0028	2.505	0.0025	2.473	0.0017	2.480
$10f_0 - f_m$	25.085 773	−20.99	−1.26	17.14	−1.6	−0.1	0.7	0.0026	0.317	0.0021	0.344	0.0015	6.220
$2f_m$	0.120 874	−2.57	9.02	2.30	−0.7	2.0	0.3	0.0098	0.335	0.0075	0.281	0.0046	0.314
$f_0 + 2f_m$	2.635 495	−67.85	−55.18	−39.37	−8.2	−6.5	−3.9	0.0042	3.216	0.0041	3.317	0.0035	3.499
$2f_0 + 2f_m$	5.150 116	−8.37	−7.21	7.53	−1.0	−0.6	0.5	0.0040	2.666	0.0030	2.502	0.0021	2.788
$3f_0 + 2f_m$	7.664 737	9.36	7.87	8.36	2.6	1.7	1.4	0.0098	1.678	0.0077	1.551	0.0057	1.512
$4f_0 + 2f_m$	10.179 358	−15.74	−7.40	−5.63	−4.3	−1.6	−0.7	0.0096	5.573	0.0075	5.564	0.0043	5.694
$5f_0 + 2f_m$	12.693 979	−4.61	2.84	0.86	−1.3	0.6	0.1	0.0095	4.162	0.0074	4.114	0.0049	4.172
$6f_0 + 2f_m$	15.208 600	−23.02	−17.53	2.52	−4.2	−2.4	0.2	0.0063	2.356	0.0048	2.413	0.0033	2.384
$7f_0 + 2f_m$	17.723 221	−7.92	−0.82	15.79	−1.1	−0.1	1.2	0.0048	0.682	0.0042	0.605	0.0025	0.709
$8f_0 + 2f_m$	20.237 842	−16.68	−18.22	−16.96	−1.6	−1.4	−0.7	0.0033	5.142	0.0026	4.945	0.0013	4.876
$9f_0 + 2f_m$	22.752 463	15.03	17.07	18.32	1.0	0.8	0.5	0.0022	3.303	0.0016	3.363	0.0010	2.844
$f_0 - 2f_m$	2.393 747	−2.16	2.55	9.01	−0.3	0.3	0.8	0.0054	5.786	0.0044	5.790	0.0030	5.570
$2f_0 - 2f_m$	4.908 368	−15.89	−4.45	−17.27	−3.5	−0.7	−1.6	0.0077	5.134	0.0053	5.054	0.0033	5.351
$^*3f_0 - 2f_m$	7.422 989	38.74	37.12	78.85	2.9	1.8	2.3	0.0026	3.328	0.0017	3.572	0.0010	3.798
$4f_0 - 2f_m$	9.937 610	−67.38	−63.91	−68.81	−7.3	−5.4	−3.4	0.0038	1.956	0.0029	1.977	0.0017	2.160
$^*5f_0 - 2f_m$	12.452 231	−49.39	−56.33	−70.03	−3.1	−2.7	−2.7	0.0022	0.680	0.0016	0.445	0.0013	0.793
$^*6f_0 - 2f_m$	14.966 852	−112.05	−123.78	−101.45	−4.4	−4.4	−2.2	0.0014	4.630	0.0012	4.592	0.0008	4.714
$^*7f_0 - 2f_m$	17.481 473	−88.32	−94.99	−28.84	−3.5	−3.0	−0.7	0.0014	3.053	0.0011	3.028	0.0008	2.882
$f_0 + 4f_m$	2.756 369	8.49	33.32	8.55	1.8	5.3	1.0	0.0073	5.385	0.0055	5.408	0.0040	5.620
$2f_0 + 4f_m$	5.270 990	10.58	32.28	23.18	1.2	2.9	1.5	0.0040	3.604	0.0031	3.664	0.0022	3.654
$f_0 - 4f_m$	2.272 873	98.12	41.49	70.76	7.6	3.7	3.6	0.0027	1.948	0.0031	2.402	0.0018	2.443
$2f_0 - 4f_m$	4.787 494	50.96	54.76	−3.99	6.0	3.8	−0.2	0.0041	5.921	0.0024	5.884	0.0021	6.080
$^*3f_0 - 4f_m$	7.302 115	88.66	90.46	97.93	7.5	5.1	4.0	0.0029	5.100	0.0020	4.930	0.0014	5.341
$f_0 + 12.5f_m$	3.270 084	−45.30	−20.18	−12.27	−3.7	−1.7	−0.8	0.0028	3.050	0.0030	2.960	0.0024	2.956
$2f_0 - 12.5f_m$	4.273 780	9.48	39.58	50.07	1.2	3.7	2.4	0.0044	3.821	0.0033	3.783	0.0017	4.018
$^*2f_0 + 12.5f_m$	5.784 705	−143.83	−36.28	−101.75	−9.4	−2.8	−5.3	0.0023	1.096	0.0026	1.336	0.0018	1.599
$3f_0 - 12.5f_m$	6.788 401	−17.73	−74.47	−28.12	−2.6	−9.0	−2.1	0.0051	2.557	0.0042	2.473	0.0025	2.346

Table 5 – *continued*

Frequency ID	Frequency (cd^{-1})	$\Delta f(B)$	$\Delta f(V)$ (10^{-5} cd^{-1})	$\Delta f(I_C)$	$\Delta f/\sigma_f$ B	$\Delta f/\sigma_f$ V	$\Delta f/\sigma_f$ I_C	$A(B)$ (mag)	Φ (B) (rad)	$A(V)$ (mag)	Φ (V) (rad)	$A(I_C)$ (mag)	Φ (I_C) (rad)
$f_0 - f'_m$	2.512 651	30.64	39.23	25.88	7.1	5.2	2.4	0.0081	2.906	0.0046	2.718	0.0033	2.567
$2f_0 - f'_m$	5.027 272	29.86	−12.99	−99.47	4.4	−1.5	−5.9	0.0051	0.709	0.0039	0.484	0.0020	0.600
$3f_0 - f'_m$	7.541 893	7.10	−4.20	−48.85	0.8	−0.5	−3.2	0.0038	5.460	0.0039	5.365	0.0023	5.214
f'_m	0.001 970	110.33	196.07	195.70	11.4	12.4	9.3	0.0036	0.717	0.0022	0.539	0.0016	0.127

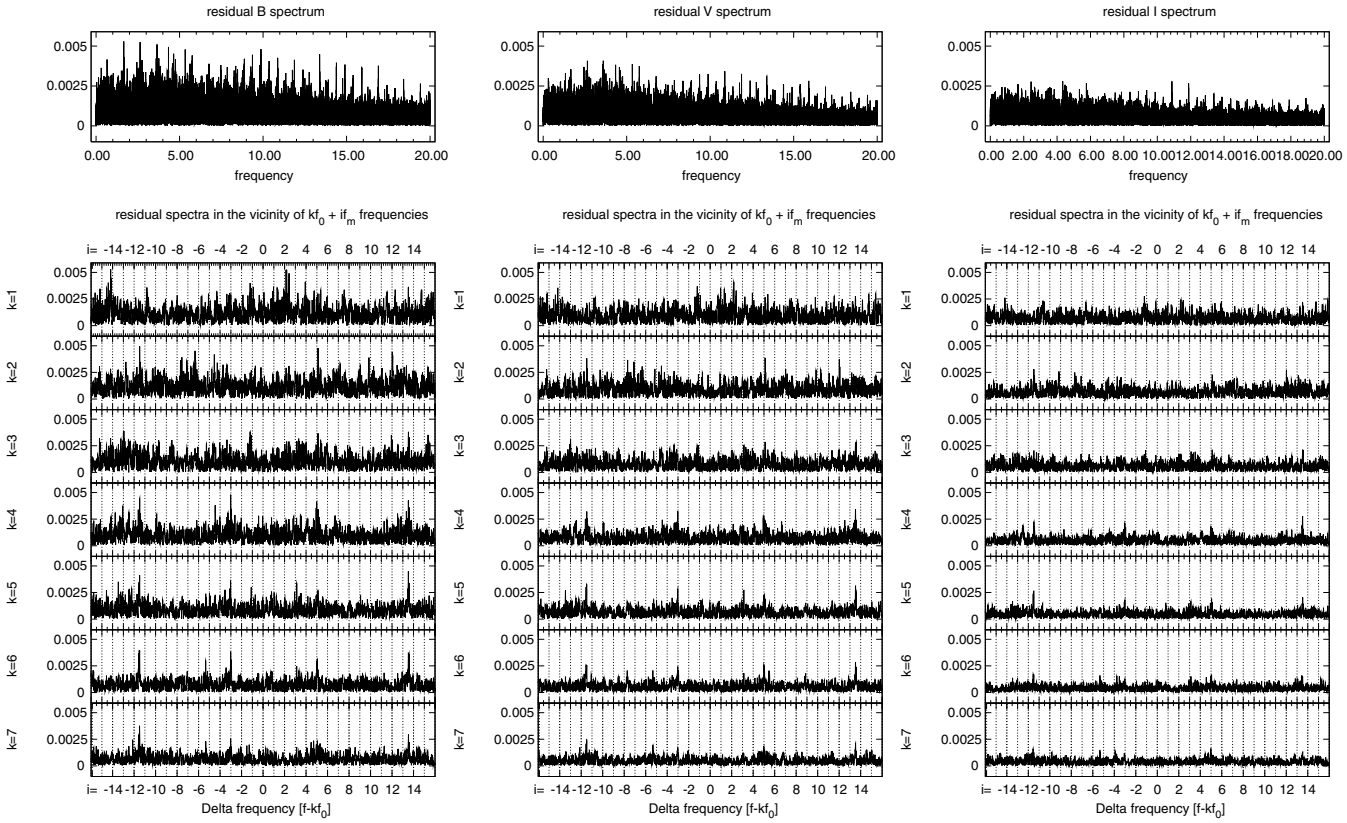

Figure 5. The top panels show the residual spectra of the B, V and I_C data pre-whitened with frequency solution D (septuplet frequencies and modulation components with $12.5f_m$ and f'_m separations). The spectra are zoomed in the vicinity of the kf_0 frequencies $k = 1, \ldots, 7$ in the bottom panels. Not regarding the decreasing mean level of the spectra towards longer wavelengths the residuals are similar, peaks at $-3f_m, 5f_m, -11.5f_m$ and $13.5f_m$ can be identified. Further significant peaks appear in the $|\Delta f| < 3f_m$ vicinity of f_0. Though it is very probable that many of these frequencies are real signals we stop with frequency identifications here as the addition of these components does not significantly improve the light-curve solution.

D in the vicinity of the given frequency) smaller than 3 in each band are denoted by asterisks. The inclusion of these frequencies in the light-curve solution has minimal effect on the results. However, as we are focusing on how accurately the light curve of a Blazhko variable can be fitted with the mathematical model of equidistant modulation side frequencies, we decided to include these low S/N signals also in the frequency solution.

The rms scatter of the residual light curves of light-curve solution D in the B, V and I_C bands are 0.026, 0.020 and 0.015 mag, respectively. Comparing these rms values to the residuals of the comparison–check stars' light curves, which are in the 0.008–0.015 mag range it seems that the residual scatter of MW Lyr is significantly larger than expected. The V magnitudes of MW Lyr vary between 12.95 and 14.35 mag, the brightnesses of the check stars C1, C2 and C3 nearly equal to the variables maximum, mean and minimum brightnesses, respectively (see the magnitudes and colours of the comparison and check stars in Table 1). The mean $\Delta(B - V)$ between MW Lyr and C0 is −0.25 mag, while the $\Delta(B - V)$ colour differences of the three check stars are between 0.02 and 0.28 mag. Neither the brightness nor the colour differences can account for the larger scatter of the residual light curve of MW Lyr.

Fig. 6 shows some examples how light-curve solutions A, B and D fit the observations on different nights. It can be seen that the observations deviate systematically even from the fit of solution D that involves 66 frequency components. The deviations are systematic, they are centred on the minimum-rising branch-maximum phase of the pulsation with different shapes. The residual mimics the behaviour of the large amplitude modulation on a much smaller scale, but without any definite periodicity.

Just for a trial we have included further 30 frequencies in the fit (consecutive pre-whitening with the highest peaks appearing in

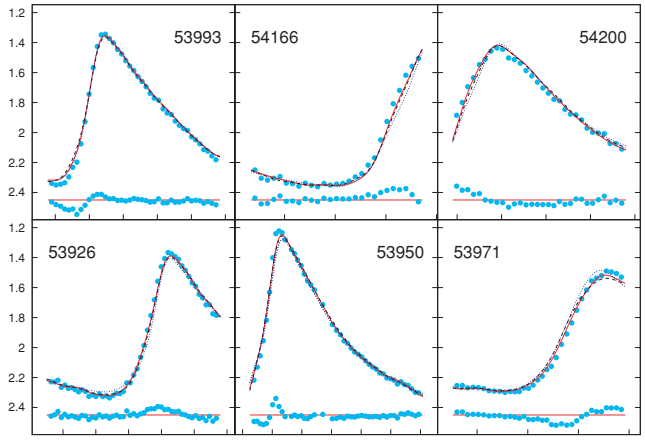

Figure 6. *V* light curves and the triplet (dotted blue line), quintuplet (dashed black line) and light-curve solution D (solid red line) fits to the data are shown on some representative nights. On the *x*-axes tick marks are at 0.005 d on each plot. Bellow the light curves the residuals if light-curve solution D is removed are shown. The residuals show smooth light curves with systematic deviations from zero. Large residuals appear at around minimum and maximum light and on the rising branch. However, as e.g. on JD 245 4200 the residual is continuously small but negative on the upper part of the descending branch. These systematic deviations explain the large rms scatter of the residual light curve.

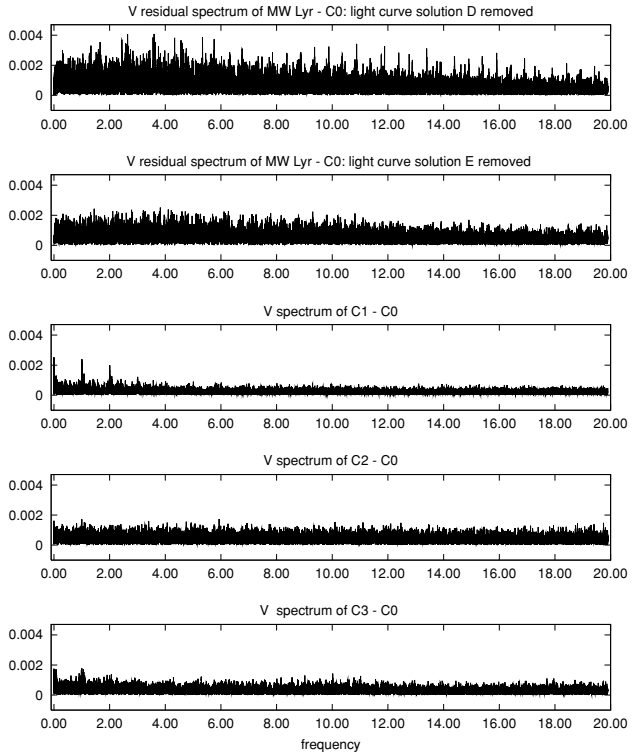

Figure 7. Comparison of the residual spectra of the *V* light curve of MW Lyr with the spectra of the check stars' light curves. The identifications and magnitudes of the C0 comparison and C1, C2, C3 check stars are given in Table 1. Two residual spectra of MW Lyr are shown. After removing the 66 frequencies of light-curve solution D significant peaks in the spectrum still appear (see also Fig. 5). Removing further 30 frequencies from the data the residual spectrum is still at two–three times higher level than the noise spectrum of the check stars. As the brightness of MW Lyr varies between 13.10 and 14.30 mag, while C1, C2 and C3 have brightnesses of 12.99, 13.92 and 14.36 mag, respectively, brightness differences cannot account for the large residual signal of MW Lyr.

the spectra shown in Fig. 5, light-curve solution E) to see whether these systematic deviations can or cannot be eliminated with further distinct frequency components. Though the rms of e.g. the *V* light curve has been reduced to 0.018 mag this way, the systematic deviations of the light curves shown in Fig. 6 have hardly decreased.

Fig. 7 compares the residual spectra of the *V* light curve prewhitened with light-curve solution D and E with the spectra of the *V* light curves of the C1, C2 and C3 check stars. The differences are striking. The mean level of the residual spectrum of light-curve solution E is still two–three times larger than that of the spectra of the check stars.

Most probably stochastic and/or chaotic behaviour of the modulation bring forth the enhanced residual signals. It seems that the light curves of large modulation amplitude Blazhko variables cannot be modelled with the required accuracy with the Fourier sum of finite number of frequency components.

3.2 The maximum brightness–maximum phase variation

The modulation of the pulsation light curve of MW Lyr can be also followed using the maximum brightness, maximum phase data given in Table 3. The maximum brightness and maximum phase values of the *V* light curve are shown in the left-hand panels of Fig. 8 folded with the modulation period. None of these plots can be fitted with a single sine wave. The maximum phase data show a highly asymmetric shape, while there is a bump on the rising branch of the maximum brightness data. For an accurate fit, both plots need at least sixth-order Fourier sums. Table 6 lists the amplitudes of the sixth-order Fourier components of the maximum brightness and maximum phase fits. The amplitudes change with increasing order, they follow a similar trend for the maximum brightness data as the amplitudes of the sidelobe frequencies of the Fourier spectrum of the light curve do: the first-, second- and fourth-order components have pronounced amplitudes while the amplitudes of the third-, fifth- and sixth-order components are small. On the contrary, the amplitudes of the third-, fourth- and fifth-order components of the maximum phase fit are very similar. The 0.022 mag and 0.0066 phase (0.0026 d) rms scatter of the residuals of the maximum brightness and maximum phase fits are, however, too large as we estimate that the data are accurate within ± 0.02 mag and ± 0.0025 d, respectively.

The residual spectra of the maximum brightness and maximum phase data pre-whitened with the sixth-order fits of the modulation frequency are shown in the right-hand panels of Fig. 8. The residual spectrum of the maximum brightness data shows a peak with 0.015 mag amplitude at $0.7559\,\mathrm{cd}^{-1}$. This frequency equals within the uncertainty to the $0.7555\,\mathrm{cd}^{-1}$ frequency value of $12.5f_\mathrm{m}$. Though this modulation component itself does not appear in the spectrum of the light curve, it has measurable amplitudes at the $kf_0 \pm 12.5f_\mathrm{m}$ sidelobe positions as discussed in the previous section. There is no sign of this modulation component in the maximum phase data. Accordingly, the modulation connected to the $12.5f_\mathrm{m}$ frequency is dominantly amplitude modulation.

The removal of the $12.5f_\mathrm{m}$ component from the maximum brightness data lowers the residual scatter to 0.020 mag only, which is still too high to be explained with observational inaccuracy. Both the maximum brightness and maximum phase data reflect the imperfection of modelling the modulation using the Fourier sum of discrete frequency components. Most probably the observations

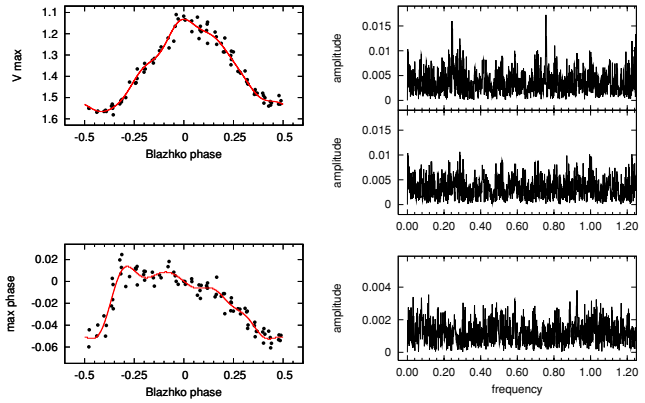

Figure 8. Maximum V brightness and maximum phase values versus Blazhko phase are plotted in the top left-hand and bottom left-hand panels, respectively. Sixth order Fourier fits to the data are also drawn in these plots. The data are pre-whitened with these fits. The top right-hand panel shows the amplitude spectrum of the residual of the maximum brightness data. The highest peak appears at $f = 0.7559\,\mathrm{cd}^{-1}$, which equals to $12.5\,f_\mathrm{m}$ within the uncertainty. Pre-whitening the data also with this frequency, there is no further significant peak in the residual spectrum (middle right-hand panel). The residual spectrum of the pre-whitened maximum phase data (bottom right-hand panel) does not show the $f = 0.7557\,\mathrm{cd}^{-1}$ signal. There is no peak appearing at the same frequency in the maximum phase residual (pre-whitened with the modulation frequency and its harmonics) and the maximum brightness residual (pre-whitened with the modulation frequency and its harmonics plus $12.5 f_\mathrm{m}$) spectra.

Table 6. Fourier amplitudes of the fits to the maximum brightness and maximum phase data.

Frequency	Maximum brightness amp (mag)	Maximum phase amp (pulsation phase)
f_m	0.2044	0.0293
$2f_\mathrm{m}$	0.0158	0.0113
$3f_\mathrm{m}$	0.0063	0.0041
$4f_\mathrm{m}$	0.0112	0.0047
$5f_\mathrm{m}$	0.0058	0.0034
$6f_\mathrm{m}$	0.0042	0.0016
$12.5f_\mathrm{m}$	0.0125	–
	rms = 0.0203	rms = 0.0066

cannot be traced with the expected accuracy using finite number of strictly periodic signals.

Plotting the maximum brightness versus maximum phase data, as Fig. 9 shows, significant scatter appears around a triangular shape curve. No evolution of the data with time account for the scatter, data from different segments of the observations are equally scattered without any systematics. Synthetic maximum brightness and maximum phase curves are drawn according to the triplet light-curve solution, light-curve solution D and maximum brightness and maximum phase fits involving six harmonics of the modulation and $12.5\,f_\mathrm{m}$ for the maximum brightness data in the panels I, II and III in Fig. 9, respectively. Many observed maximum data are out of the ranges of any of the model fits, that cannot be explained by data inaccuracy.

3.3 The mean light curve

Interesting questions arise in connection with the mean light curves of variables showing light-curve modulation. Namely, we still do not know whether

(a) the mean light curve is or is not the same as the light curve of a star with the same physical parameters but not showing Blazhko modulation,

(b) the actual shape of the light curve in any phase of the modulation corresponds to the mean light curve.

Our extended and accurate data make it possible to find the correct answers to these questions. However, first we have to define the mean pulsation light curve of Blazhko variables correctly.

The simplest way to define the mean light curve is to fit all the data with a high enough order Fourier sum of the pulsation frequency and its harmonics (method a). However, this procedure may yield a mean light curve that is biased by the uneven data sampling, even in the case of an extended data set. The typical procedure of light-curve analysis of Blazhko stars is pre-whitening first with the pulsation frequency and its harmonics (with the mean light curve defined above), and then, the pre-whitened data are analysed to identify the modulation components. As a result of the incorrect shape of the removed mean light curve during this procedure false signals in the vicinity of the pulsation components emerge. A better approximation of the mean light curve is gained by a fit that takes the pulsation and modulation frequency components simultaneously

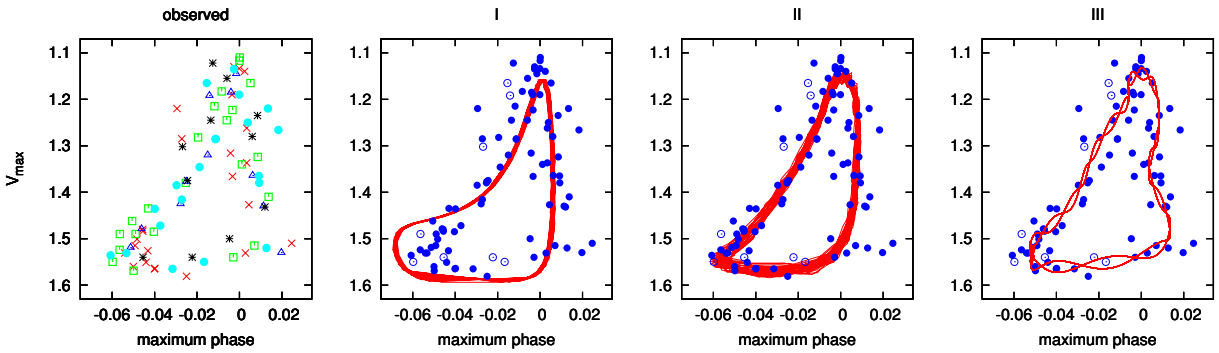

Figure 9. V maximum brightness versus maximum phase data of the 88 observed maxima. Data for the consecutive 50–70 d segments (three–five Blazhko cycles) are shown by different symbols in the left-hand panel. No systematic change with time in the V_max–$\mathrm{Phase}_\mathrm{max}$ plot is evident. For comparison, in the I, and II panels synthetic V_max–$\mathrm{Phase}_\mathrm{max}$ curves according to the light-curve solution A (triplet) and D (that involves the septuplet solution of the modulation plus four modulation components with $12.5\,f_\mathrm{m}$ separation, and four modulation components with $f'_\mathrm{m} = 0.0019\,\mathrm{cd}^{-1}$ modulation frequency) are plotted. In panel III the fitted curve corresponds to the harmonic fits to the maximum brightness and maximum phase data with the frequencies given in Table 6. The observed V_max–$\mathrm{Phase}_\mathrm{max}$ data are overplotted on the synthetic solutions, the open symbols denote less accurate data. The scatter of the observations is much larger than observational uncertainties can explain as data are accurate within ± 0.02 mag and ± 0.003 d, ± 0.0075 phase ranges.

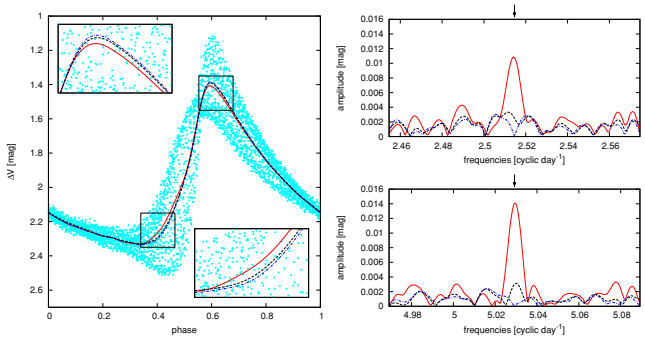

Figure 10. Comparison of the mean light curves defined as (a) the Fourier fit of the pulsation frequency and its harmonics to the *V* observations from the first season (solid red line); (b) the Fourier parameters of the pulsation components are taken from a triplet solution of the data of the first season (dashed black line); (c) the Fourier parameters of the pulsation components are taken from light-curve solution D of the entire data set (blue dot–dashed line). The residual spectra in the vicinity of the pulsation frequency and its first harmonic component are shown in the right-hand panels. In method (a) the modulation side components are also removed but in a second step after the pulsation frequencies have been already removed from the data. Note the smaller amplitude of the fitted light curve and the high residual signals at f_0 and $2f_0$ when applying method (a).

into account. The mean pulsation light curve according to a triplet solution light-curve fit (method b) may significantly differ from the mean light curve defined by method (a).

Fig. 10 demonstrates the differences between the fits and the residual spectra if the data are fitted and pre-whitened by the pulsation and modulation components in consecutive steps and simultaneously. In this figure data from the first season of the observations are shown. This data set, which contains 3900 data points from 120 nights is, however, more dense and extended than any previous photometric observation of a Blazhko variable. Though these data cover the whole pulsation light curve in each 0.05 phase of the modulation, the differences between the mean light curves defined by method (a), and by method (b) are significant.

The fitted mean light curves shown in Fig 10 are

(i) the Fourier fit to the data with the pulsation frequency and its harmonics (method a);

(ii) the fit taken from the simultaneous triplet frequency solution of the data (method b);

(iii) the pulsation light curve taken from the complete light-curve solution of the entire data set (light-curve solution D as given in Table 5).

Method (a) gives substantially smaller amplitude around minimum and maximum light due to the oversampling of the small amplitude phase of the modulation in the data, than the fits either from method (b) or from the light-curve solution D. The latter fits are very similar, showing that with the inclusion of the most prominent modulation components (triplets) in the light-curve solution quite a reliable mean light curve can be gained even if the data sampling is biased.

The right-hand panels in Fig. 10 show the residual spectra of the three fits in the vicinity of the pulsation frequency and its first harmonic. In order to make the residuals comparable, the modulation side frequencies are also removed in a second step in method (a). These residual spectra show high amplitude signals at f_0 and $2f_0$, which also points to the inadequacy of pre-whitening the data in consecutive steps.

We thus conclude that one has to be cautious how to define the mean light curve of a Blazhko variable as from method (a) and method (b) different results emerge. In real observations data sampling is always somewhat unevenly distributed. As a consequence, the mean light curve defined without taking the modulation components also into account, may give an incorrect result for variables showing any type of light-curve modulation.

From here on, we use the Fourier parameters of the pulsation components given in Table 5 to define the mean pulsation light curve.

3.4 Light curve changes during the Blazhko cycle

Utilizing the full coverage of the pulsation period in each phase of the modulation in our data set we can reliably compare the mean light curve to the light curves in different phases of the Blazhko modulation. In Fig. 11 the *V* light curves of MW Lyr are shown for 20 bins of the modulation cycle. The scatter of these light curves can be partially explained by the regular light curve changes that take place even in 0.05 phase intervals of the modulation. Modulation frequencies that are not integer multiplets of f_m (e.g. $12.5f_m$ and f'_m) also result in enhanced scatter of the data phased with the modulation period. Moreover, our experience, that the light curve cannot be fitted with the required accuracy supposing regular modulations with different modulation periods as discussed in Sections 3.1 and 3.2, means that this irregular character of the modulation adds some extra noise to the light curves in the different phase bins, as well.

Notwithstanding these effects, the light curves in the different phase bins are well defined, and can be characterized by the Fourier amplitudes and phases of the pulsation frequency and its harmonics.

The changes in the Fourier amplitudes and phases (phase differences) of f_0 and its lower harmonics and also the average values of these parameters are listed in Table 7. For comparison, the last line gives the corresponding parameters of the mean *V* light curve. The first five columns in Table 7 give the phase bin, the order of the Fourier sum fitted to the data, the residual scatter of the fit, the intensity weighted mean magnitude and the number of data points belonging to the given bin, respectively. The phases of the f_0 pulsation frequency can be read from the sixth column (initial epoch is 2 453 887.00) while the next four columns list the epoch independent phase differences $\Phi_{k1}(k = 2, \ldots, 5)$. The amplitudes of the kf_0 $(k = 1, \ldots, 5)$ components are given in the last five columns. The residual scatters of the fitted harmonic functions to the data in the different phase bins of the modulation are within the 0.015–0.032 mag range. The average of the rms values of the fits is 0.022 mag, slightly larger than the rms of the light-curve solution D of the entire data set.

The data listed in Table 7 and plotted in Fig. 12 show that there are major differences between the Fourier parameters of the mean light curve (the Fourier parameters of the kf_0 components of the full light-curve solution given in Table 5) and the average values of the same Fourier parameters of the light-curve fits in different phases of the Blazhko cycle. The amplitudes of the kf_0 components of the mean light curve are systematically 0.01–0.02 mag smaller than the averages derived from the fits of the individual light curves. The $\Phi_{21}, \Phi_{31}, \Phi_{41}$ and Φ_{51} phase differences of the mean light-curve solution are 0.16, 0.17, 0.35 and 0.78 rad smaller than the averages of the corresponding parameters of the light curves in different phases of the Blazhko cycle.

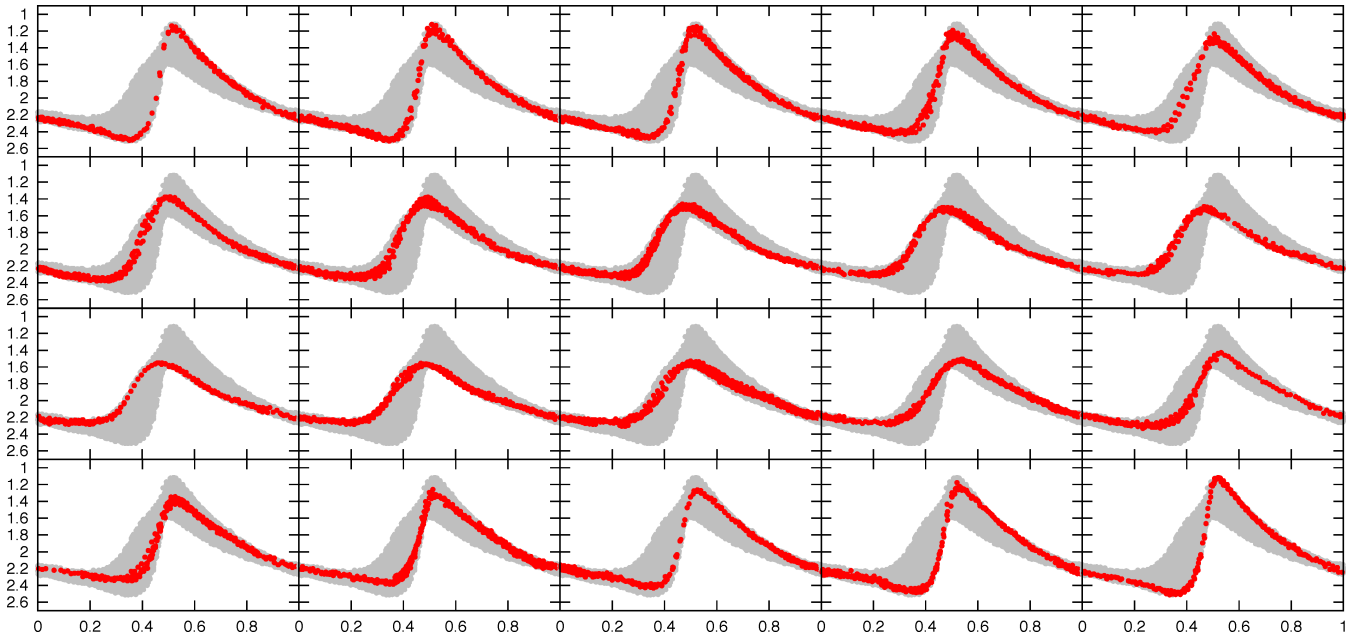

Figure 11. *V* light curves of MW Lyr in 20 different phases of the Blazhko cycle are shown. The folded light curve of the complete data set is shown in grey colour.

Table 7. Fourier parameters of the *V* light curves in the 0.05 phase bins of the modulation.

Bl phase	Order	rms	$\langle V \rangle$	N	$\Phi(f_0)$ (rad)	Φ_{21}	Φ_{31}	Φ_{41}	Φ_{51}	$A(f_0)$	$A(2f_0)$	$A(3f_0)$ (mag)	$A(4f_0)$	$A(5f_0)$
0.00–0.05	14	0.015	2.031	228	1.691	2.423	5.173	1.483	4.146	0.459	0.244	0.148	0.092	0.059
0.05–0.10	14	0.024	2.024	277	1.737	2.430	5.136	1.465	4.166	0.460	0.247	0.142	0.087	0.052
0.10–0.15	13	0.032	2.017	294	1.792	2.417	5.095	1.364	3.980	0.457	0.234	0.130	0.077	0.047
0.15–0.20	13	0.020	2.011	347	1.866	2.438	5.024	1.342	3.824	0.441	0.209	0.108	0.060	0.033
0.20–0.25	13	0.019	2.006	285	1.965	2.449	5.030	1.285	3.800	0.421	0.197	0.087	0.042	0.019
0.25–0.30	13	0.026	2.005	341	2.053	2.452	5.018	1.462	4.074	0.394	0.176	0.078	0.041	0.018
0.30–0.35	13	0.026	2.003	352	2.155	2.416	5.023	1.426	4.278	0.369	0.156	0.066	0.035	0.014
0.35–0.40	12	0.022	2.006	376	2.210	2.386	5.067	1.597	4.371	0.349	0.149	0.059	0.031	0.014
0.40–0.45	11	0.019	2.007	280	2.274	2.440	4.978	1.600	4.114	0.333	0.132	0.051	0.023	0.012
0.45–0.50	9	0.026	2.003	147	2.266	2.501	4.913	1.789	4.262	0.331	0.127	0.059	0.023	0.008
0.50–0.55	9	0.016	1.999	194	2.309	2.453	4.858	1.543	4.501	0.308	0.118	0.049	0.019	0.008
0.55–0.60	9	0.016	2.000	303	2.240	2.446	4.906	1.196	3.270	0.296	0.109	0.049	0.010	0.002
0.60–0.65	9	0.022	1.993	381	2.083	2.445	5.046	1.115	3.910	0.312	0.103	0.052	0.016	0.005
0.65–0.70	6	0.018	1.990	338	1.938	2.433	5.104	1.136	3.755	0.333	0.117	0.052	0.018	0.007
0.70–0.75	8	0.027	1.995	192	1.816	2.443	5.054	1.073	3.838	0.355	0.146	0.065	0.035	0.016
0.75–0.80	9	0.027	2.004	288	1.770	2.323	5.016	1.283	3.729	0.368	0.177	0.093	0.054	0.033
0.80–0.85	10	0.025	2.009	376	1.737	2.346	5.075	1.342	3.850	0.392	0.189	0.102	0.068	0.037
0.85–0.90	11	0.018	2.012	268	1.681	2.392	5.105	1.467	4.096	0.416	0.215	0.121	0.077	0.043
0.90–0.95	13	0.025	2.028	277	1.650	2.386	5.196	1.501	4.220	0.442	0.239	0.140	0.080	0.055
0.95–1.00	15	0.015	2.026	252	1.676	2.447	5.141	1.453	4.094	0.462	0.250	0.154	0.094	0.065
Average values														
0.00–1.00	11	0.022	2.008	290	1.946	2.423	5.046	1.395	4.014	0.385	0.177	0.090	0.049	0.027
Parameters of the light-curve solution given in Table 5 (mean light curve)														
0.00–1.00	12	0.020	1.966	5796	1.919	2.262	4.878	0.943	3.239	0.374	0.159	0.076	0.037	0.020
Parameters of the mean light curve of the time transformed data														
0.00–1.00	13	0.020	2.008	5796	1.955	2.417	5.068	1.405	4.034	0.384	0.176	0.089	0.049	0.027

These large differences make it unambiguous that in each phase of the Blazhko modulation the light curve of MW Lyr differs from its mean light curve.

The Φ_{k1} phase differences show quite a surprising behaviour. In spite of the large amplitude of the Blazhko modulation of MW Lyr, Φ_{21} and Φ_{31} hardly vary, while the changes in Φ_{41} and Φ_{51} show complex behaviour with cycle length half of the modulation cycle. For the higher order components the amplitudes at around Blazhko minimum are so small that the errors in the phases become too large to make any firm conclusion about their variations.

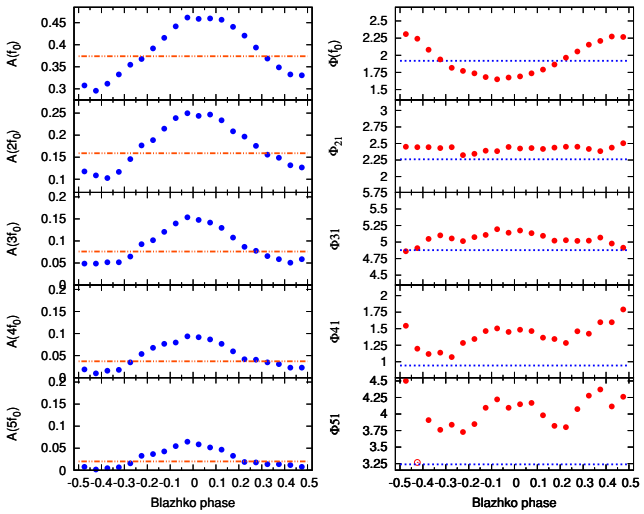

Figure 12. Fourier parameters of the V light curves in 20 phase bins of the Blazhko cycle are plotted. The open circle in the Φ_{51} plot denotes a very uncertain data point, the amplitude of the $5f_0$ component is only 0.002 mag in this phase bin. The amplitudes and the phases are plotted on the same scales. Note that the Fourier phases have opposite sign as the directly measured phase of the maximum brightness shown in Fig 8. The amplitudes of the kf_0 ($k = 1 \ldots, 5$) components and the $\Phi(f_0)$ phase show smooth, sinusoidal variations with the smallest phase value when the amplitudes are the highest and with the largest phase value when the amplitudes are the smallest. On the contrary the epoch independent phase differences (Φ_{k1}) show surprisingly different behaviour. There are small if any changes in Φ_{21}, and the variation in Φ_{31} is also very small taking into account the significant changes in the light curves' shapes as shown in Fig. 11. Φ_{41} and Φ_{51} vary during the Blazhko cycle showing complex changes on the time-scale of about half the modulation period. For comparison, Fourier parameters of the mean light curve as given in Table 5 are also drawn by dashed lines in the plots. While the $\Phi(f_0)$ value of the mean light is close to the average of their observed values in the different Blazhko phases, the phase differences in each phase of the modulation are larger than the phase differences of the mean light curve. The Fourier amplitudes of the mean light curve are 0.01–0.02 mag fainter than the averages of their values in different phases of the Blazhko cycle.

The light curve changes during the Blazhko cycle can be summarized as follows.

Light curve changes connected to the amplitude variations.

The amplitudes of the kf_0 frequencies show parallel changes but the amplitudes of the higher order components decrease more drastically than the amplitudes of the lower order components. For example, the amplitude ratio $A(f_0)/A(f_5)$ is about 7 in the three largest amplitude phase bins, but this ratio is as large as 50–150 for the three smallest amplitude phase bins.

The light curves at around maximum amplitude phase of the modulation can be fitted accurately with 10–15 harmonic components of f_0. The light curves are much more sinusoidal in the small amplitude phases, they can be fitted with six–nine harmonic components with the required accuracy.

Light curve changes connected to the phase variations.

The phases of the lower order harmonic components show much harmonized changes as indicated by the small variations of the lower order phase differences. This means that the changes in the light curves' phase can be characterized basically by one parameter, with the phase of the f_0 pulsation frequency, $\Phi(f_0)$.

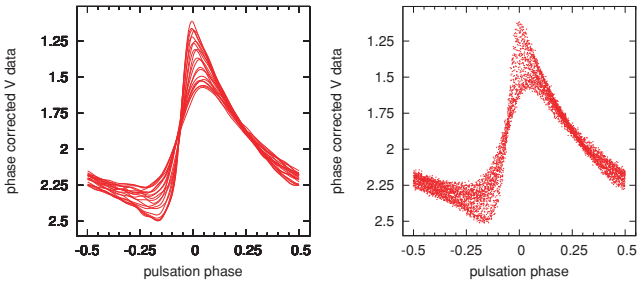

Figure 13. Left-hand panel: fitted curves of the V light curve of MW Lyr in 20 bins of the Blazhko cycle. Each light curve is phase shifted with the $\Phi(f_0)$ phase value. Right-hand panel: time transformed V light curve of MW Lyr. The time transformation was defined from a second-order harmonic fit to the $\Phi(f_0)$ phases in different phases of the modulation.

The Φ_{41} and Φ_{51} phase differences show double wave curves indicating that the time-scale of their variation is about half of the period of the modulation. The appearance of the $2f_m, 4f_m$ frequency components in the Fourier spectrum of the whole data set is probably connected with this double periodic behaviour of the higher order phase differences.

We have also tested how accurately the observations can be fitted with a simple mathematical model which describes the amplitude and phase changes of the different order pulsation components with different order Fourier series. We have found that such a light-curve solution fails to fit the observations with similar accuracy as the Fourier sum of the pulsation and modulation side lobe frequencies involving even a smaller number of parameters. This result means that the modulation has a very complex behaviour that could not be described by a mathematical model of amplitude and phase modulations of harmonic functions.

Phenomenologically, amplitude modulation occurs if there are observed changes in the brightnesses of the light-curve maxima, while phase modulation manifests itself as a missing fix point on the rising branch of the folded light curve.

Exploiting the slight changes in the lower order phase differences, we can 'harmonize' the phases of the light curves with a simple phase correction. Shifting the fitted light curves of the different bins by their $\Phi(f_0)$ values a surprisingly coherent light-curve series emerge as shown in Fig. 13. The pronounced fix point occurring on the rising branch in this figure validates our simple treatment separating the phase modulation of the light curve from the amplitude modulation by correcting the phases with the $\Phi(f_0)$ values.

A similar procedure can be applied on the whole data set, as well. Fitting the $\Phi(f_0)$ values of the 20 phase bins with a second order Fourier sum we can define a continuous function of the phase variation. It is supposed that by transforming the times of the observations according to this function we 'get rid of' the phase modulation component of the modulation. As the right-hand panel in Fig. 13 shows, this is indeed the case, the light curve of the time transformed data shows very regular amplitude modulation with a pronounced fix point on its rising branch. The phase difference of the amplitude peaks of the time transformed data is much smaller than in the original data. Its range is consistent with the value expected from the amplitude variation.

Without starting the light-curve analysis from the beginning using this phase-corrected data set, we have only checked

(i) whether or not the same frequency components occur in the spectrum of the time transformed data as in the original data set, and

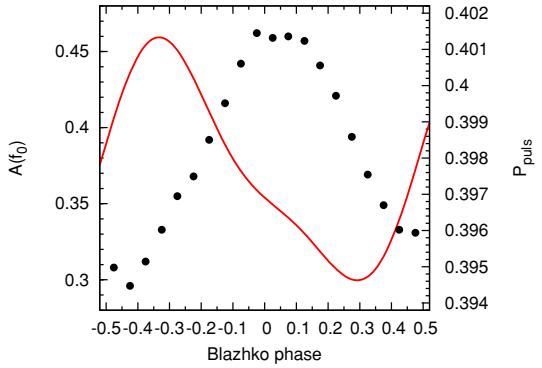

Figure 14. Phase relation of the amplitude (dots) and period (red line) changes of MW Lyr during the Blazhko cycle. The amplitude and period variations are measured as the amplitude and as the derivative of the phase variation of the f_0 pulsation frequency component, respectively.

(ii) how the rms scatter of the time transformed data compares to the rms residual of the original data.

All the frequencies but $2f_0 - 4f_m$ and $3f_0 - 4f_m$ listed in Table 5 can be identified in the residual spectrum of the time transformed data. The f_m and $2f_m$ modulation sidelobe components can be detected up to higher order harmonics as contrasted with the spectrum of the original data.

The residual scatter of the original *V* light curve was 0.020 mag, the rms scatter of the time transformed data remains the same, 0.020 mag if the modulation components up to the appropriate order are taken into account. The Fourier parameters of the mean pulsation light curve of the time transformed data (given in the last line in Table 7) equal within their error ranges with the average values of the Fourier parameters of the observed light curves in different phases of the Blazhko cycle. The residual light curve of the time transformed data also shows large deviations at around minimum-rising branch-maximum phases of the pulsation.

Without finding the correct explanation of the Blazhko phenomenon we cannot decide which characterization of the light curve is correct: the Fourier analysis of the light curve as it is, or the separation of the phase and amplitude modulation components of the light-curve modulation by an appropriate transformation of the phases (times) of the observations. The simplicity and the low number of independent parameters involved in the time transformation applied suggest that this new treatment of the light curve may lead to a headway in the study of Blazhko variables.

We also remark that the time transformation can be explained as a continuous change in the pulsation period during the Blazhko cycle as Stothers (2006) has also interpreted. The full range of period change determined from the derivative of the phase shift curve is 0.006 d, i.e. $\delta P/P = 0.015$. The period of the pulsation is about 0.401 d around Blazhko phase 0.65 and 0.395 d around Blazhko phase 0.30 as Fig. 14 shows. The amplitude of the period variation is somewhat larger than Stothers (2006) derived for RR Lyr itself, but keeping in mind that for RR Lyr temporal periods were determined for some days long intervals of the observations, most probably a reduced value of its real period change was found.

4 CONCLUSIONS

The photometric observations of MW Lyr analysed in this paper comprise the most extended and accurate data set of a Blazhko variable ever obtained. Utilizing this unique opportunity a detailed and circumspect phenomenological description of the modulation is given, which may provide crucial information to find the correct explanation of the phenomenon.

The main results and conclusions of the analysis are the followings.

(i) In the Fourier spectrum of the light curve besides the $kf_0 \pm f_m$ triplet frequencies $kf_0 \pm 2f_m$ quintuplet and $kf_0 \pm 4f_m$ septuplet components also appear.

(ii) Both f_m and $2f_m$ frequencies can be detected in the spectrum.

(iii) Frequency components at $kf_0 \pm 12.5f_m$ are detected. If these frequencies are not 'just by chance' at $\pm 12.5f_m$ separations but somehow they are indeed connected to the main modulation frequency, then it is a great challenge to find an answer to their origin.

(iv) Modulation with $12.5f_m$ frequency can also be detected in the maximum brightness data but not in the maximum phase observations. Consequently, the modulation connected to the $12.5f_m$ frequency is dominantly amplitude modulation.

(v) Stothers (2006) mentioned the lack of large amplitude modulation around minimum phase of the pulsation as a failure of his model. The amplitude of the modulation around minimum phase of the pulsation in MW Lyr is, however, commensurable with the amplitude of the modulation in maximum brightness. On the contrary, the modulation of MW Lyr is more strictly periodic and regular than it would be expected to be if the triggering mechanism behind the modulation were the cyclic weakening and strengthening of the turbulent convection in the ionization zones as Stothers (2006) proposes.

(vi) Though the modulation shows high degree of regularity both in the phase (period) and in the amplitude changes, the light curve cannot be fitted with the required accuracy even with 66 identified and further 30 frequencies appearing in the residual spectrum. Significant deviations in the residual light curve are concentrated at the minimum-rising branch-maximum phase of the pulsation. These residuals, however, do not show any periodicity, most probably they can be explained with some stochastic and/or chaotic behaviour of the modulation itself.

(vii) The mean pulsation light curve defined by the Fourier parameters of the kf_0 pulsation frequency components of the full light-curve solution differs significantly from the light curve in any phase of the modulation. Especially the Φ_{k1} phase differences of the mean light curve are discrepant, they are out of the range of the phase difference values measured in any phase of the Blazhko cycle.

(viii) The light curves in the small and large amplitude phases of the modulation can be fitted with 6–10 and 11–15 order harmonic fits, respectively. If non-linear effects (e.g. shock waves) account for the occurrence of the higher order harmonic components of the pulsation, then their diminishing amplitudes in the low amplitude phase of the modulation may indicate that these non-linear effects are not so important in this phase of the modulation.

(ix) Stothers (2006) proposed that the enhanced convection lowers the pulsation amplitude in the small amplitude phase of the modulation, while the phase relation between the period changes and the amplitude variations depends on the physical parameters of the individual variable in a complex way. The pulsation period of MW Lyr is the longest about 1–2 d (0.1 phases of the modulation cycle) later than the minimal amplitude phase, while it is the shortest about 3–4 d (0.2 phases of the modulation cycle) later than the maximal amplitude phase.

(x) The small variations in the phase differences of the lower order harmonic components of the light curves during the Blazhko

cycle indicate that the phase variations of these frequency components are very coherent. If the modulation were caused by the interaction of close radial mode and non-radial mode frequencies (Dziembowski & Mizerski 2004), then no such phase coherency would be expected.

(xi) The modulation of the light curve of MW Lyr can be separated into amplitude and phase modulation components using only one parameter, the phase of the f_0 pulsation frequency in each phase bins of the modulation. This is in agreement with the explanation of the Blazhko effect with period and amplitude changes as recently proposed by Stothers (2006).

It would also be important to know how common the detected properties of the light-curve modulation of MW Lyr are. Only further similar observations of other Blazhko stars can give an answer to this question.

ACKNOWLEDGMENTS

We wish to thank the referee, Hiromoto Shibahashi, for his useful comments that helped us to improve the paper. This research has made use of the SIMBAD data base, operated at CDS Strasbourg, France. The financial support of OTKA grants K-68626 and T-048961 is acknowledged. HAS thanks the US National Science Foundation for support under grants AST 0440061 and AST 0607249.

REFERENCES

Dziembowski W. A., Mizerski T., 2004, Acta Astron., 54, 363
Gessner H., 1966, Veroeff. Sternwarte Sonnberg, 7, 61
Hurta Z., Jurcsik J., Szeidl B., Sódor Á., 2008, AJ, 135, 957
Jurcsik J. et al., 2005, A&A, 430, 1049
Jurcsik J. et al., 2006, AJ, 132, 61
Kolenberg K. et al., 2006, A&A, 459, 577
Kolláth Z., 1990, Occ. Techn. Notes Konkoly Obs., No. 1, http://www.konkoly.hu/staff/kollath/mufran.html
Kolláth Z., Csubry Z., 2006, Mem. Soc. Astron. Ital., 77, 109
Mandel O. E., 1970, Perem. Zvezdy, 17, 335
Montgomery M. H., O'Donoghue D., 1999, Delta Scuti Star Newsl., 19
Shibahashi H., 2000, in Szabados L., Kurtz D. W., eds, ASP Conf. Ser. Vol. 203, The Impact of Large-Scale Surveys on Pulsating Star Research. Astron. Soc. Pac., San Francisco, p. 299
Smith H. A., 1995, RR Lyrae Stars. Cambridge Univ. Press, Cambridge
Smith H. A., Barnett M., Silbermann N. A., Gay P., 1999, AJ, 118, 572
Sódor Á., 2007, Astron. Nachr., 328, 829
Sódor Á., Jurcsik J., 2005, Inf. Bull. Var. Stars, 5641
Stothers R., 2006, ApJ, 652, 643

SUPPORTING INFORMATION

Additional Supporting Information may be found in the online version of this article:

Table S1. Photometric $BV(RI)_C$ sequence in the field of MW Lyr (A. Henden).
Table 2. Time series of the V magnitude and colour differences of MW Lyr relative to the comparison star C0 (GSC2.2 N0223233663).
Table S2a. ΔB time series.
Table S2b. ΔR_C time series.
Table S2c. ΔI_C time series.
Table 3. Maximum timings and brightness values derived from the V light curve.

Please note: Wiley-Blackwell is not responsible for the content or functionality of any supporting information supplied by the authors. Any queries (other than missing material) should be directed to the corresponding author for the article.

This paper has been typeset from a TEX/LATEX file prepared by the author.